TURBULENT CHARACTERISTICS OVER A ROUGH NATURAL SURFACE
PART I: TURBULENT STRUCTURES

FAZU CHEN*

Flinders Institute for Marine and Atmospheric Research, Adelaide, S.A., Australia

(Received in final form 29 January, 1990)

Abstract. A comprehensive experiment for turbulence and profiles has been carried out over a very rough natural mallee bushland. In Part I, the large inherent structures of the turbulence are presented. Short-period space-time correlations of wind and temperature indicate that periodic fluctuations pervade the lower surface layer above the canopy. These are associated with the appearance of large turbulent structures. Prominent peaks in the spectra are identified with the arrival of these structures, which show that they have a relatively large length scale over rough surfaces. These findings suggest a different mechanism for the enhancement of turbulent diffusivity over rough surfaces from that by the simple generation of turbulence by plant wakes.

Analysis via conditional sampling of the turbulent components has revealed that 'bursts' make almost the same contributions as 'gusts' (at the measurement height of 8.4 m above ground) for either momentum or temperature under neutral conditions; for unstable conditions and high 'hole' size H (see Equation (3)), gusts dominate for momentum while bursts dominate for heat transfer. This implies that the mechanisms for momentum and heat transfer are different.

1. Introduction

Much work during the last ten years (Garratt, 1978; Raupach, 1979; Denmead and Bradley, 1985) has shown that there are distinct anomalies in flux-gradient relationships over forest. In a recent experiment, Chen (1987) and Chen and Schwerdtfeger (1989) have made detailed investigations of the roughness transition layer in the atmospheric surface boundary layer over a rough natural bushland. They found that violations of the conventional flux-gradient relationships may be related to turbulent structures.

Large coherent turbulent structures have been extensively studied in laboratory boundary layers (see for example the reviews by Willmarth, 1975 and Kovasznay, 1977). Conditional sampling (e.g., Kovasznay *et al.*, 1970), together with flow visualization and long-established space-time correlation techniques, have shown that within the apparent chaos of a turbulent boundary layer, there exist large, coherent structures distributed randomly in time and in the horizontal plane, with length scales ranging from some surface-defined scale l_s to the boundary-layer thickness δ, and with finite lifetimes long enough for coherence to be preserved over streamwise distances of 10δ to 20δ.

It has been shown that the smooth-wall region is characterized by a randomly

* Present Address: Institute of Geography, Chinese Academy of Sciences, Beijing 100101, China.

Boundary-Layer Meteorology **52**: 151–175, 1990.

recurring 'burst cycle' in which low-speed fluid near the wall is ejected violently into the overlying flow, immediately followed in time by a downsweep of higher-speed fluid into the region close to the wall (e.g., Kim *et al.*, 1971; Nychas *et al.*, 1973); also, intense, intermittent Reynolds-stress contributions and turbulent production rates are associated with these 'ejection' (or 'burst') and 'sweep' events (e.g., Wallace *et al.*, 1972; Lu and Willmarth, 1973). For rough surfaces, there are only a few published studies (e.g. Grass, 1971; Nakagawa and Nezu, 1977; Raupach *et al.*, 1980), which show that (close to rough surfaces or within canopies) sweeps account for most of the stress while bursts are more influential through most of the rest of the boundary layer.

Although there are even fewer results, such structures undoubtedly also occur in the atmospheric boundary layer, and their interaction with the underlying surface is central to the nature of canopy turbulence. In the studies of Allen (1968) and Isobe (1972), it is suggested that air motions with length scales much larger than those typical of the canopy might make important contributions to the velocity field. Finnigan (1979) has shown that canopy turbulence is strongly influenced by large-scale coherent motions in the overlying boundary layer.

Part I presents the results of a study of the structures of turbulence over the rough natural surface of the Hincks mallee-bushland. Spectra and space-time correlations are used to exhibit the different scales of the eddies. Contributions of different parts of the turbulence spectrum to momentum and heat transfer are investigated by means of conditionally sampled quadrant analysis.

2. Experimental Site and Instrumentation

The experiments were performed in the western part of the Hincks Conservation Park in the central Eyre Peninsula of South Australia. The climatology of this area has been described by Schwerdtfeger (1985). The Hincks Park has a width of 40 km in the east-west direction and extends 25 km from north to south, thereby providing a 12–20 km flat and uniform fetch around the site within the directional range of 32–270°. The vegetation is characteristic of natural mallee bushland (dominant species *Euc. diversifolia*). The ground cover consists of low bushes and kangaroo grass (*Themeda Australia*) about 0.5–1.0 m high. The overall canopy structure was determined mainly by aerial photography, using a ground-based

TABLE I

Surface characteristics at Hincks Park

Mean canopy height, h	2.3 m
Mean spacing, D	5.0 m
Mean width, l	3.5
Mean density, λ	0.32 m
Roughness length, z_0	0.435 m
Zero-plane displacement, d	1.8 m

survey around the site for reference. The estimated values of canopy structure parameters are shown in Table I.

2.1. Eddy covariance measurements

Instantaneous vertical and horizontal wind speeds were measured with a Gill propeller anemometer manufactured by the R. M. Young Company. Fluctuations in temperature were measured by unshielded tiny thermistor beads of type U-23 manufactured by STC. Although a small error due to lack of radiation shielding was expected because of the minute physical size of the beads, this was considered to be insignificant in view of the main purpose of the temperature sensor, viz., to measure fluctuations in air temperature, with slow trends filtered out. The absolute error was found to be about 0.3°C under test conditions of strong sunlight (Raupach, 1976; Coppin, 1979). Since changes in radiative intensity are generally confined to frequencies well below the flux-carrying range, the absence of a radiation shield introduces no significant errors in an eddy correlation context. Fluctuations in humidity were measured by an infrared hygrometer (Raupach, 1978). The eddy covariances were determined at a height of 8.4 m above the ground and sampled at a rate of 10 Hz. Corrections to these covariances have been made for possible errors in eddy correlation measurements arising from such factors as tilt error, sensor deficiencies and high frequency loss.

2.2. Profile measurements

The 3-cup miniature anemometers designed by Bradley (1969) were used for wind profile measurements and set at heights of 2.9, 4.1, 6.7, 9.6, 13.1, 21.1 m above the ground. Temperatures were measured by means of thermistor beads of type RA53 with ventilated radiation shields of the type described by Schwerdtfeger (1976) and set at heights of 2.8, 3.9, 6.3, 9.1, 12.7, 20.7 m above the ground. The outputs of these instruments were sampled and stored every 2 sec to give almost instantaneous profile data. The linearized bridges, careful calibrations and high resolution of the analogue-digital converter ensured that the uncertainty of the temperature measurements was within 0.02 °C. In order to avoid any systematic errors involved in the profile measurements due to different characteristics between individual sensors, the wind and temperature sensors were interchanged three times during the 21 day period of observations; thus it was ensured that each sensor was used representatively over the full range of heights.

2.3. Other measurements

The improved net-radiaometer designed and built by Swissteco (type S1) was used for measuring net radiation and mounted on a separate mast of about 10 m in height. Soil heat flux was directly measured by heat flux plates, manufactured by Middleton Instruments. Three identical sensors were connected in series and buried 1 cm below the surface in locations offering contrasting exposures.

Further details regarding the site, instrumentation and corrections have been given by Chen (1987).

The energy budget equation was used to examine the reliability of the eddy measurements by comparing the eddy heat fluxes (sum of the sensible and latent heat fluxes) with the independently measured available energy (sum of the net radiant and soil conducted energy). A reasonable overall agreement between the two was obtained.

3. Statistical Characteristics of Turbulence over the Rough Surface

3.1. Spectral analysis

Spectral analysis for runs 100 and 120 are plotted in Figures 1 and 2, which represent neutral and unstable conditions, respectively. The stability parameter ξ, defined as $(z-d)/\mathscr{L}$, where z is the height above ground, d the zero plane displacement of the canopy, and $\mathscr{L}$ the Monin–Obuhkov length scale, was -0.035 and -0.461 for run 100 and run 120, respectively. Both spectra have distinct peaks in the range of 0.03 to 0.1 Hz. The predominant peaks are at higher frequencies in the neutral case, and lower frequencies in the unstable case. However, these peak frequencies are much lower than others which have been observed previously. For instance, Finnigan (1979) found a predominant peak frequency of 0.35 Hz over a wheat canopy. This discrepancy indicates that the 'active eddies' over the very rough mallee-bush surface may have an inherently large length scale. If this means that their influence extends upward a considerable distance from the rough surface that generates them, it may suggest a mechanism for the enhancement of eddy diffusivity over rough surfaces.

3.2. Space-time correlations

Space-time correlation coefficients have often been used to investigate the dependence of velocity or temperature structure on height, and from this, information about eddy features can be obtained, e.g., the periodicity in the turbulence, or length scales ranging from some surface-defined scale l_s to the boundary-layer thickness δ, space and time scale of the eddies. The space-time correlation coefficient, $R_{u_z u_r}(z, \tau)$, for velocity of u_z and u_r, is defined as

$$R_{u_z u_r}(z, \tau) = \frac{\overline{u_z'(z, t-\tau/2) \cdot u_r'(z_r, t+\tau/2)}}{(\overline{u_z'^2(z, t-\tau/2)} \cdot \overline{u_r'^2(z_r, t+\tau/2)})^{1/2}} \tag{1}$$

where u_z' is the wind speed fluctuation at height z, u_r' is the wind speed fluctuation at a reference height z_r, and τ is the time delay. The space-time correlation coefficient for temperature is similar to (1). In the computation, the reference height z_r was regarded as the top level of the six heights in the profile measurements. Three examples of wind and temperature for neutral and unstable conditions were selected to compute the correlations for a maximum time delay of

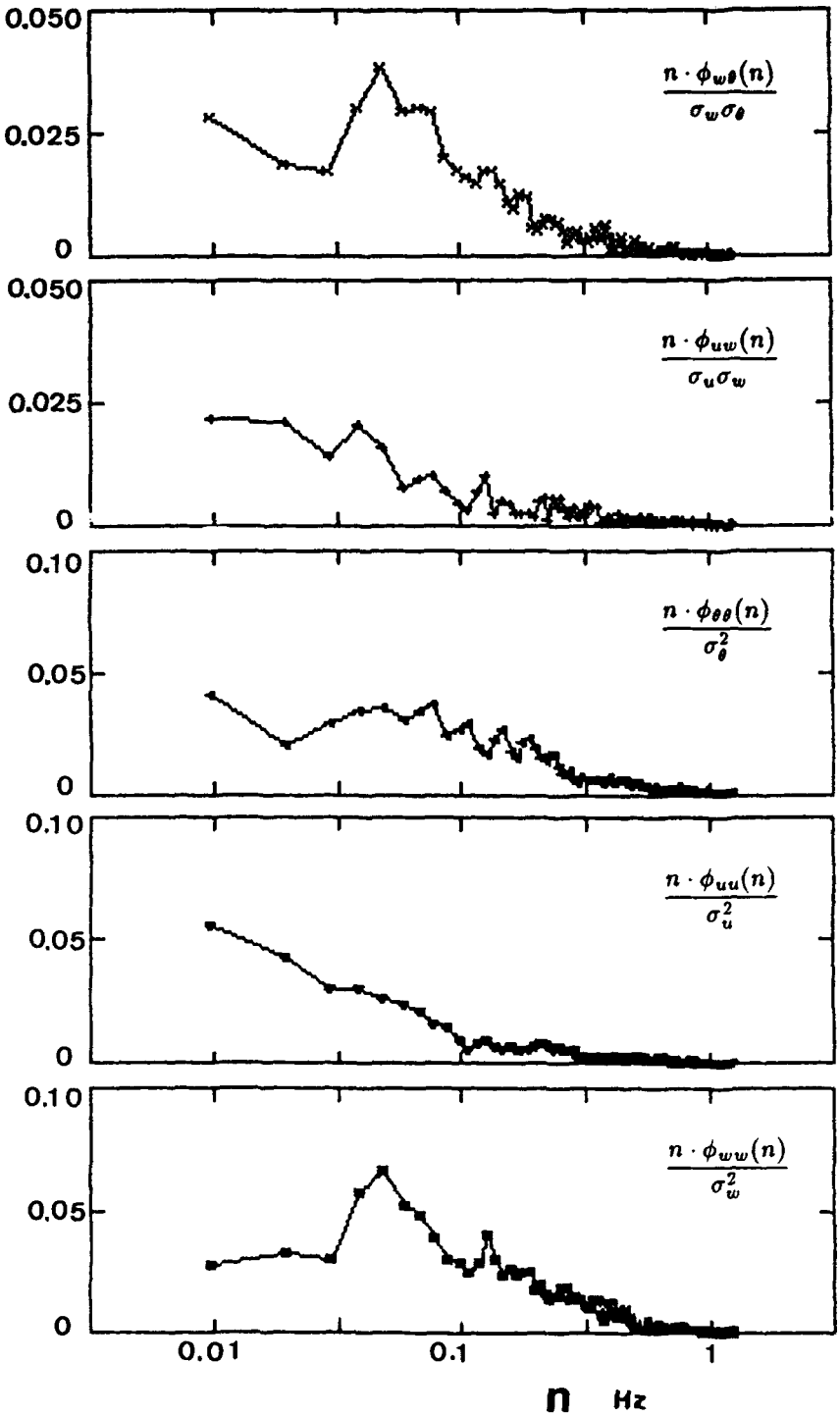

Fig. 1. Normalized power- and cospectra against frequency in neutral condition Run 100.

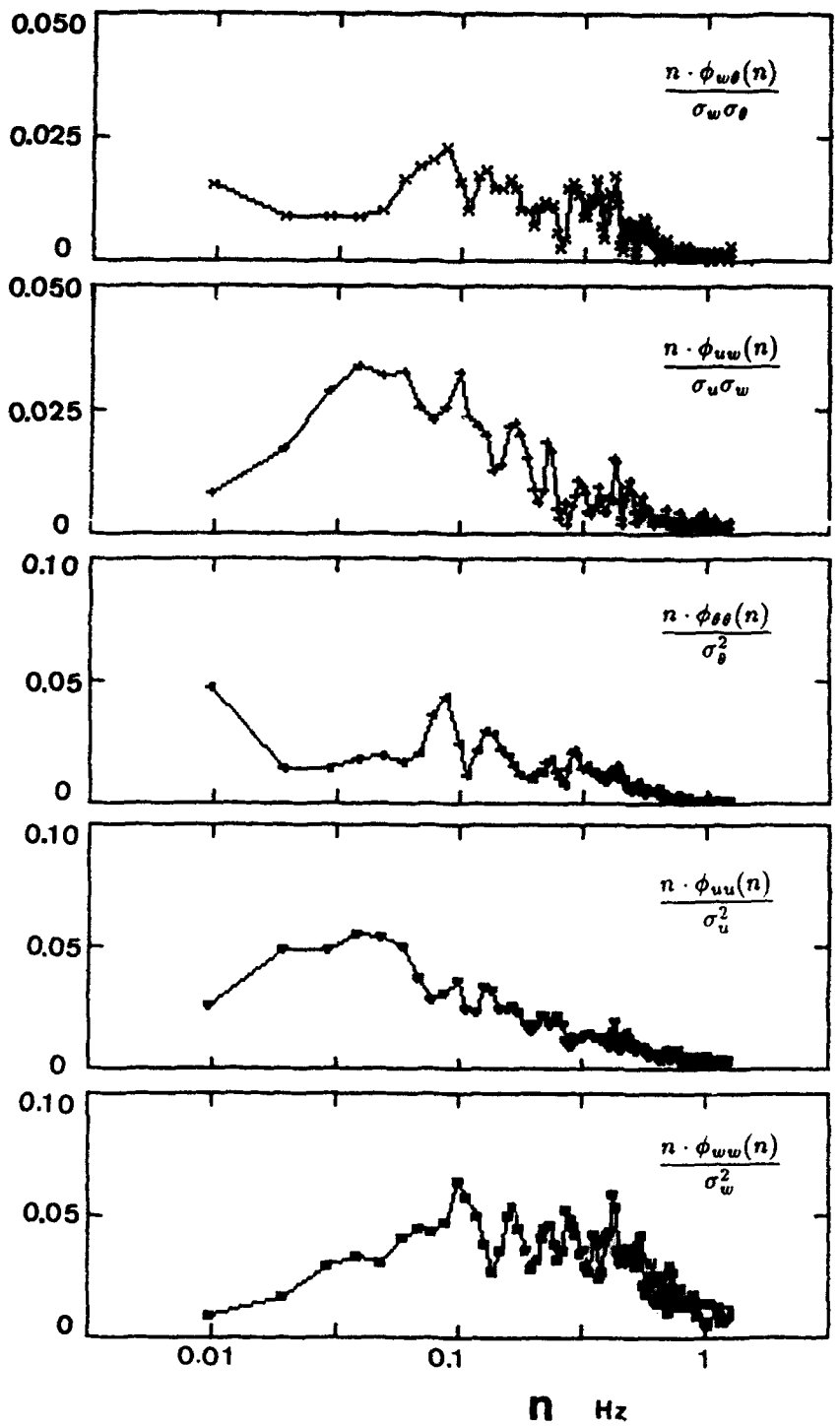

Fig. 2. Normalized power- and cospectra against frequency in unstable condition Run 120.

200 sec (the duration of the time series data is 15 min), as shown in Figures 3 and 4. In each graph, the top curve is the auto-correlation at the reference height, and the other five curves are the space-time correlations for the reference height and the other five heights. Figures 3 and 4 show high space-time correlations for

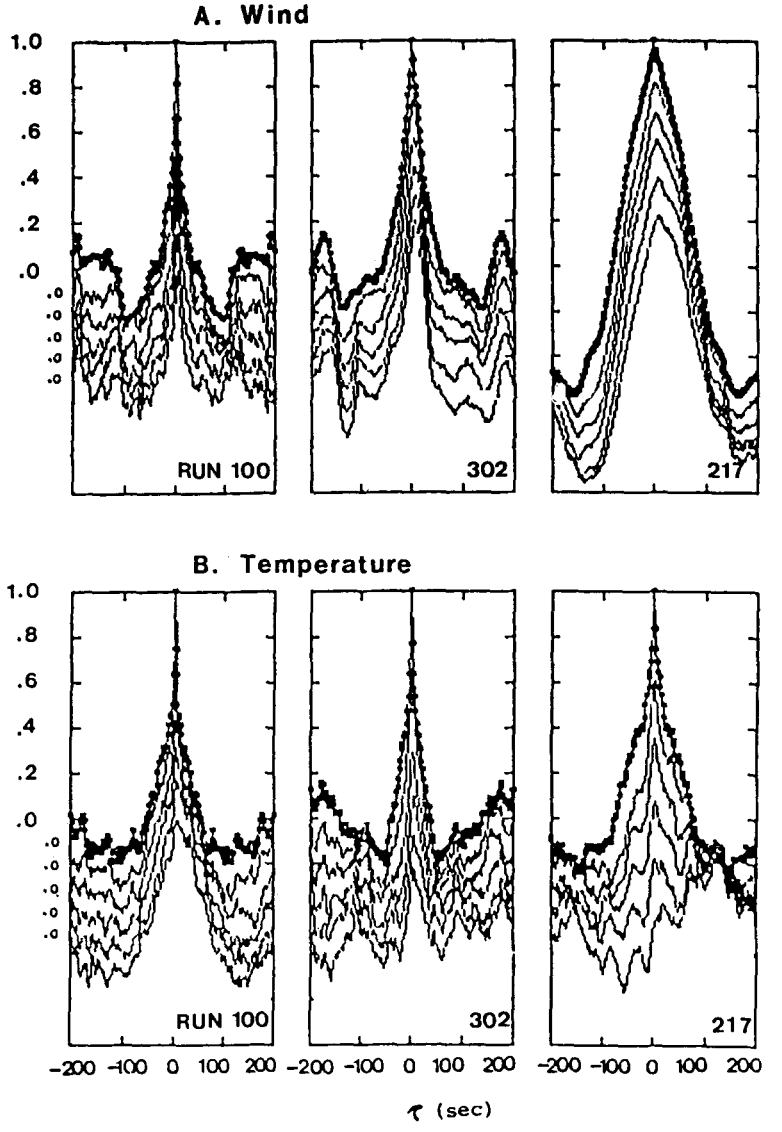

Fig. 3. Long-term space-time correlations coefficients of wind (A) and temperature (B) with a maximum time delay of 200 sec under neutral conditions for different wind speeds. Stability parameter $\zeta = -0.035$, -0.065, and -0.060, and $U = 7.8$, 5.9 and 3.5 m/s, for run 100, 302 and 217, respectively. The top trace is the auto-correlation of the 6th level and all others are the cross-correlations of the 6th level with lower levels in descending order from Figures 3 to 6, and from Figures 8 to 9. the vertical axes of each are staggered for clarity.

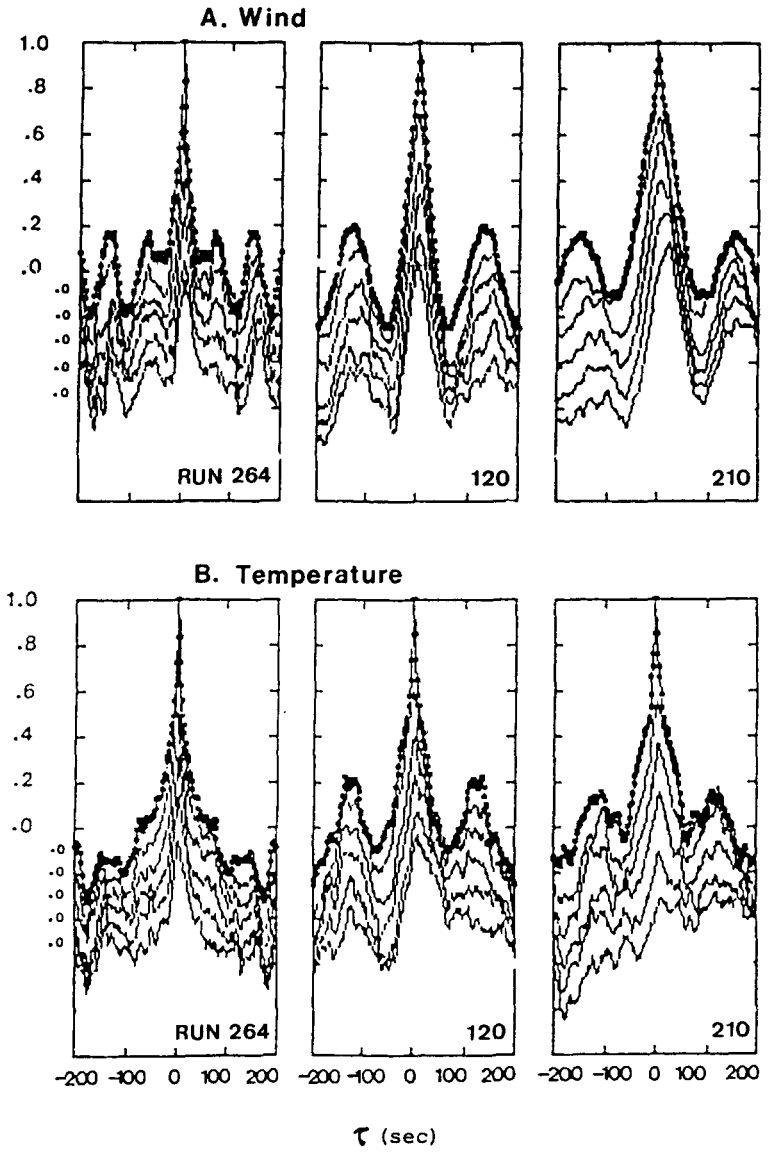

Fig. 4. The long-term space-time correlation coefficients of wind (A) and temperature (B) with a maximum time delay of 200 sec in unstable conditions for different wind speeds. $\zeta = -0.112$, -0.461 and -1.577, and $U = 6.3$, 3.0 and 2.1 m/s, for run 264, 120 and 210, respectively.

both wind and temperature under either neutral or unstable conditions. For instance, the correlations for wind between the reference height and the lowest level have values above 0.4. For a closer consideration of the peaks of maximum correlations, the data of Figures 3 and 4 are re-computed with a maximum time delay of 40 sec as shown in Figures 5 and 6. It can be seen that the peaks

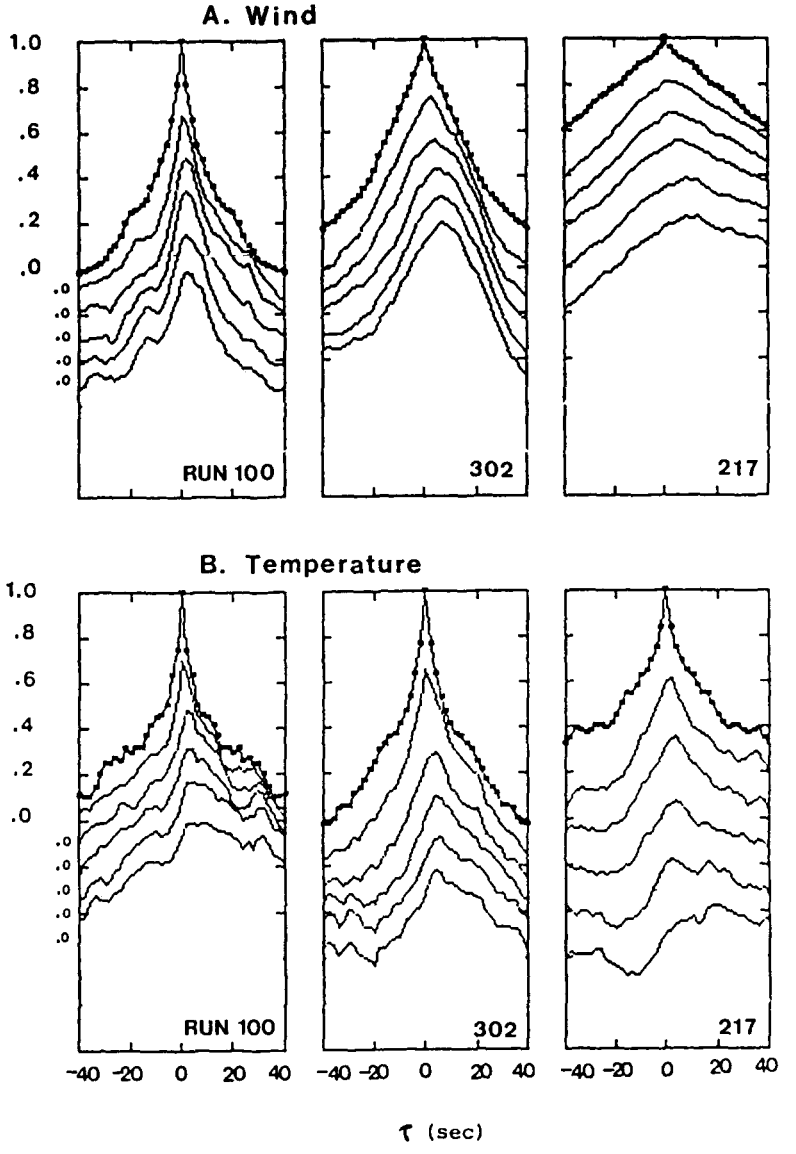

Fig. 5. Long-term space-time correlations coefficients of wind (A) and temperature (B) with a maximum time delay of 40 sec under neutral conditions for different wind speeds. Stability parameter $\zeta = -0.035$, -0.065 and -0.060, and $U = 7.8$, 5.9 and 3.5 m/s, for Run 100, 302 and 217, respectively.

shift with height, which indicates that there is a propagation process of vertical convection. For wind in Run 302, variations of the time delay τ_p of the peak of the maximum correlation with height are shown in Figure 7. If the vertical convection velocity of the peak correlation is defined as $1/(\partial\tau_p/\partial z)$, the speed with which a streamwise velocity fluctuation at the top level propagates towards the surface,

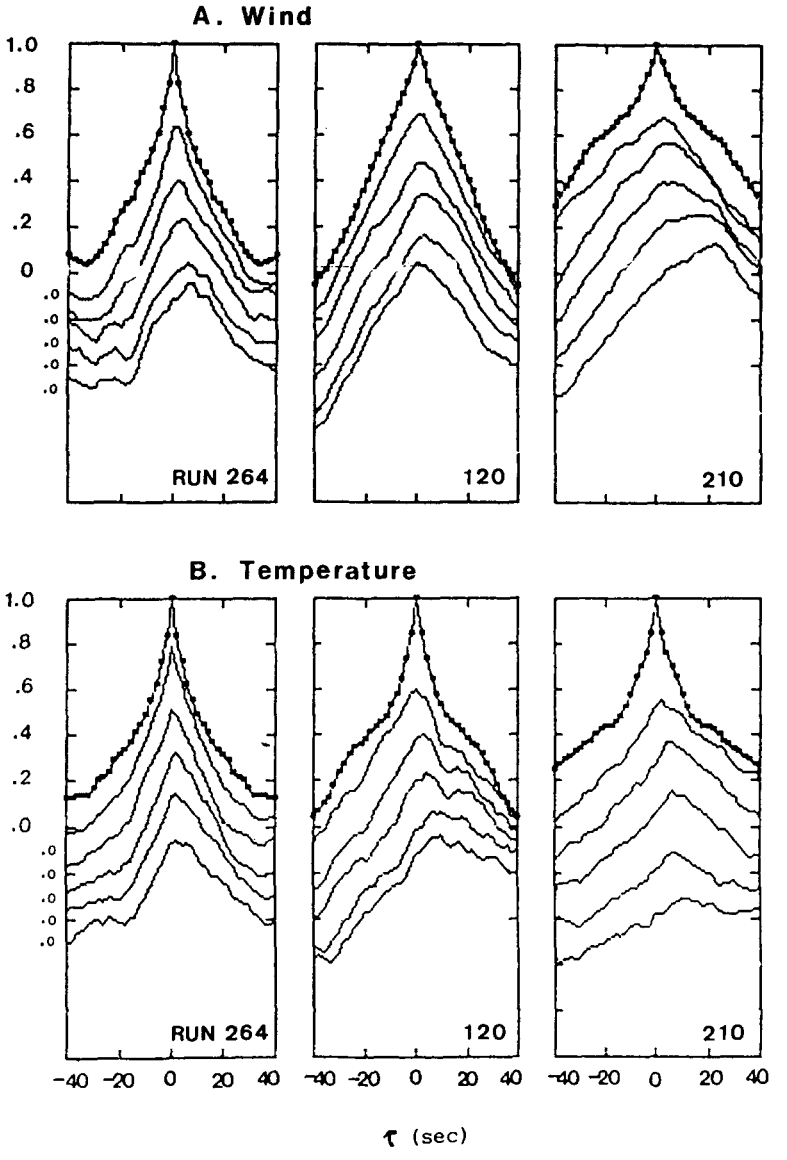

Fig. 6. The long-term space-time correlation coefficients of wind (A) and temperature (B) with a maximum time delay of 40 sec in unstable conditions for different wind speeds. $\zeta = -0.112$, -0.461 and -1.577, and $U = 6.3$, 3.0 and 2.1 m/s, for Run 264, 120 and 210, respectively.

it can be seen that the convection velocity diminishes close to surface. The curve of Figure 7 is comparable to similar data obtained over and in a wheat canopy (Finnigan, 1979) and in a laboratory wind-tunnel model (Seginer *et al.*, 1976 and Seginer and Mulhearn, 1978).

The secondary peaks in Figures 3 and 4 imply some periodic structures with

very long period cycles (typical period 100 sec). The length scales, L, of corresponding eddies could be computed from the wind velocity, U, and the time lags, τ, of secondary peaks, shown in Table II.

It seems that eddies at our site have consistent length scales of 1000–1200 m and 300–400 m for neutral and unstable conditions, respectively. Motions of this scale are probably too big to be regarded as eddies in the surface layer. They are probably a low-level manifestation in the surface layer, or mixed-layer convection cells, or possibly atmospheric gravity waves rather than turbulent phenomena on this surface-layer scale.

Thus, these shorter time period cycles in the range from 0.03 to 0.1 Hz, indicated from the spectral analysis, cannot be found in Figures 3 and 4. Their contributions must have been smoothed out in the long-time averaging involved in computing the correlations, as also pointed out by Finnigan (1979). Accordingly, the time series data have been pre-processed before re-computing space-time correlations. The time series data were divided into 30 segments; each segment had a time period of 30 sec. The fluctuation components of wind or temperature were derived by subtracting the segments' means rather than the whole time series' mean. In such a case, the short-period space-time correlations were defined as

$$\hat{R}_{u_z u_r}(z, \tau) = \frac{\overline{\overline{u''_z(z, f - \tau/2) \cdot u''_r(z_r, f + \tau/2)}}}{\left(\overline{\overline{u''^2_z(z, f - \tau/2)}} \cdot \overline{\overline{u''^2_r(z_r, f + \tau/2)}}\right)^{1/2}} \tag{2}$$

where u''_z and u''_r are fluctuating components of u_z and u_r derived by subtracting the short-time mean obtained by averaging over the periods of segments of the correlation, and the double bar '=' denotes the short-time average. As shown in Figures 8 and 9, the short-time period cycles are distinct, and the secondary peaks are located at time lags of around 20 sec under all circumstances, indicating that the predominant frequency of active eddies is around 0.05 Hz, which is expected by the spectral analyses.

3.3. Conditional sampling analysis

Turbulence has often been characterized by its intermittency and periodicity, which results from large structures. Dramatic changes of wind and temperature, and significant transfer of momentum, heat and mass could occur whenever these

TABLE II

Length scales of the eddies

Neutral				Unstable			
Run No.	U (m/s)	τ (s)	L (m)	Run No.	U (m/s)	τ (s)	L (m)
100	7.5	130	1014	264	6.3	60	378
302	5.9	180	1062	120	3.0	130	390
217	3.5	320*	1120	210	2.1	160	336

* This number is twice the time lag of the negative peak.

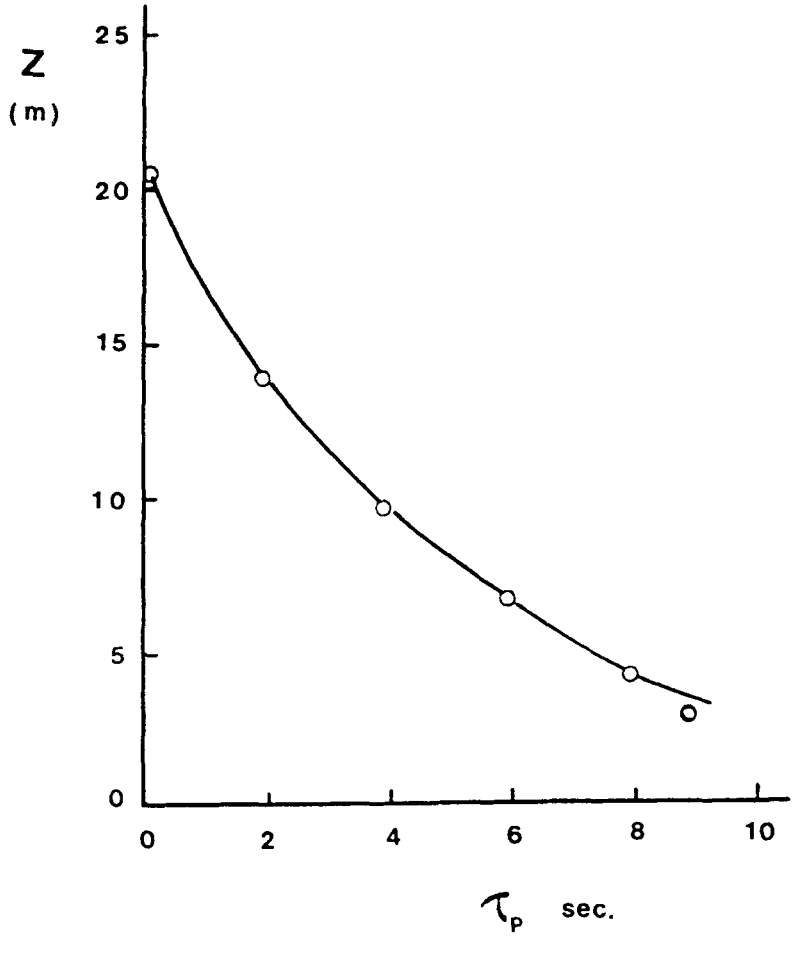

Fig. 7. The variation of the time delay τ_p of the peak of the maximum correlation for velocity with height.

large structures arrive. The parameter H, defined as

$$H = \begin{cases} u'w'/\overline{u'w'} & \text{for momentum,} \\ w'\vartheta'/\overline{w'\vartheta'} & \text{for temperature,} \end{cases} \tag{3}$$

is used as an indicator of an instantaneous momentum and heat contribution. Thus, the large structures may be defined as the events whose value of H is greater than specified values. For data of Run 100 and Run 120, the time proportions and contributions of large structures, whose value of H is greater than 4 (a value used in the present study), have been computed and listed in Table III.

Table III shows that most of the heat and momentum is transferred in a small fraction of the time. To obtain further information about the instantaneous features of the velocity and temperature fields that contribute to average shear stress

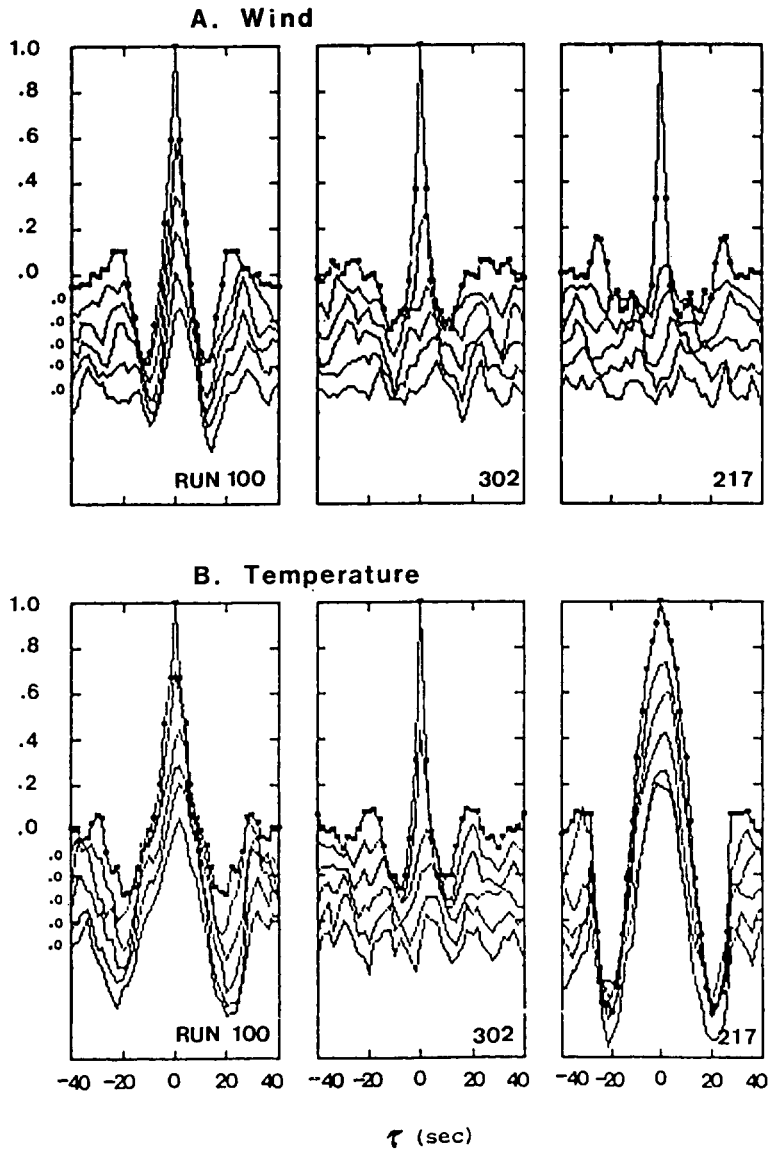

Fig. 8. The short-term space-time correlation coefficients of wind (A) and temperature (B) with a time delay of 40 sec in neutral conditions and different wind speeds.

or heat flux, quadrant analysis using the conditional sampling technique (Lu and Willmarth 1973) has been introduced, in which the contributions to $\overline{u'w'}$ or $\overline{\vartheta'w'}$ are sorted into four groups depending upon the quadrant of the $u'w'$ or $\vartheta'w'$ plane in which the correlation occurs. The four conditional averages are given below and shown in Figure 10.

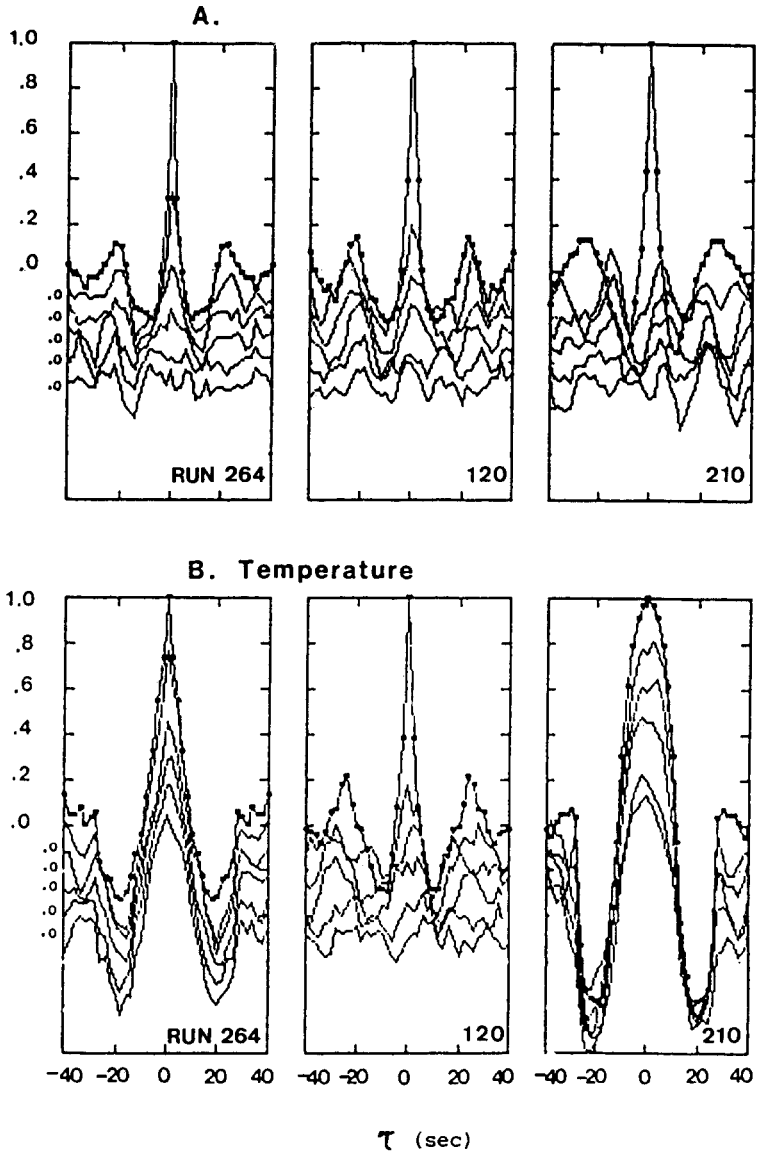

Fig. 9. The short-term space-time correlation coefficients of wind (A) and temperature (B) with a time delay of 40 sec in unstable conditions and different wind speeds.

TABLE III

Time partition and contributions of large structures

Run No.	Momentum		Heat	
	Time (%)	Momentum (%)	Time (%)	Heat flux (%)
100	9.3	54.2	9.3	52.3
120	17.3	83.1	5.1	44.5

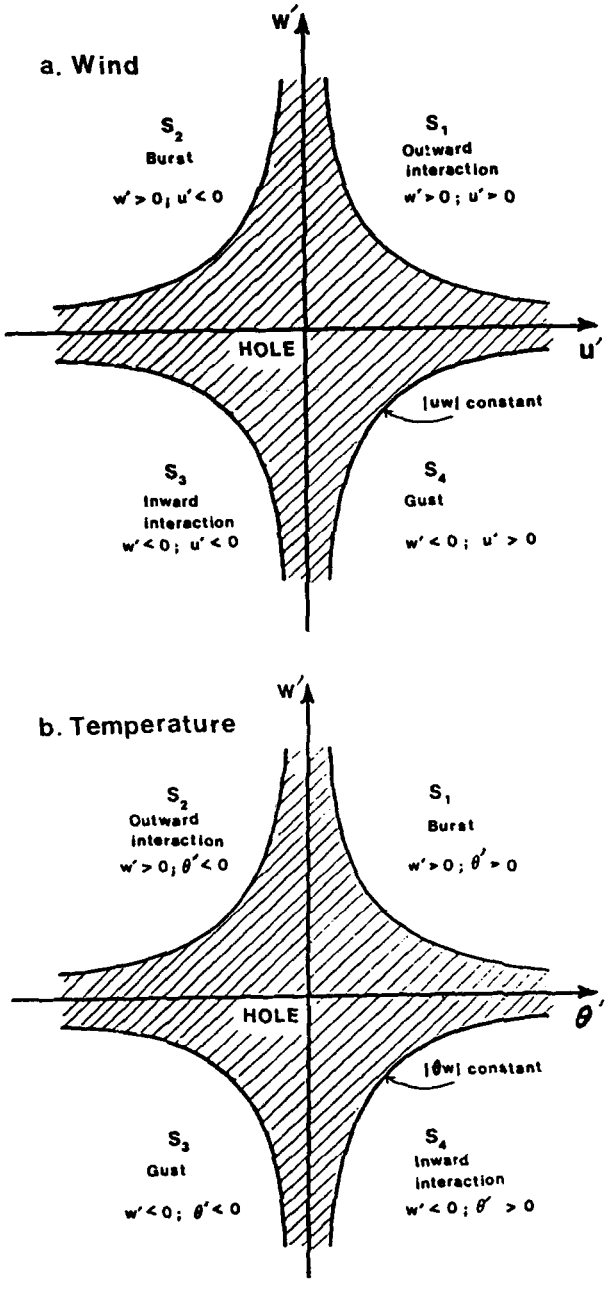

Fig. 10. Schematic drawing of the five regions of the 'quadrant' and hole' representation in $u'w'$ space (a) and $\vartheta'w'$ space (b).

For momentum:

$$S_1 = (\widehat{u'w'})_1, \quad \text{when } u' > 0, w' > 0 \text{ outward interaction;}$$
$$S_2 = (\widehat{u'w'})_2, \quad \text{when } u' < 0, w' > 0 \text{ burst;}$$
$$S_3 = (\widehat{u'w'})_3, \quad \text{when } u' < 0, w' < 0 \text{ inward interaction;}$$
$$S_4 = (\widehat{u'w'})_4, \quad \text{when } u' > 0, w' < 0 \text{ gust;}$$

for temperature:

$$S_1 = (\widehat{\vartheta'w'})_1, \quad \text{when } \vartheta' > 0, w' > 0 \text{ burst;}$$
$$S_2 = (\widehat{\vartheta'w'})_2, \quad \text{when } \vartheta' < 0, w' > 0 \text{ outward interaction;}$$
$$S_3 = (\widehat{\vartheta'w'})_3, \quad \text{when } \vartheta' < 0, w' < 0 \text{ gust;}$$
$$S_4 = (\widehat{\vartheta'w'})_4, \quad \text{when } \vartheta' > 0, w' < 0 \text{ inward interaction.}$$

where the angle bars denote a conditional average. These four conditional averages are usually normalized as

$$S_n = \frac{(\widehat{u'w'})_n}{|\overline{u'w'}|}, \quad \text{so} \quad \sum_{n=1}^{4} S_n = 1 . \tag{4}$$

Moreover, a fifth region, known as the 'hole', is added to the quadrant representation to achieve more information about the relative intermittency of the various contributions. The hole is delimited by the curves $|u'w'| = \text{constant}$. With this scheme, contributions to $\overline{u'w'}$ from each quadrant for events with H greater than some specified value can be extracted by defining $(u'w')^*_i(H)$ such that

$$\widehat{u'w'_i}^*(H) = \frac{1}{m} \sum_{k=1}^{m} \widehat{u'w'_{ik}} \cdot Y(k, H) \tag{5}$$

where $\widehat{u'w'_{ik}}$ is the kth member of the m digitized values of $\widehat{u'w'_i}$ in the ith quadrant, and the angle bars denote a conditional average with regard to H, and $Y(k, H)$ is an indicator function defined as

$$Y(k, H) = \begin{cases} 1 & \text{if } |\widehat{u'w'_{ik}}| \geq H \cdot |\overline{u'w'}| \\ 0 & \text{if } |\widehat{u'w'_{ik}}| < H \cdot |\overline{u'w'}| \end{cases} . \tag{6}$$

Figure 11 plots these four quadrant representations as functions of hole sizes, H, for momentum and temperature, for neutral and unstable conditions, respectively, and Figure 12 gives their H value contours in the four quadrant planes. It can be seen that for momentum, under neutral conditions (Run 100), gusts and bursts are almost equal in strength, and the outward and inward interactions are always small; for unstable conditions (Run 120), gusts are also equal to bursts at $H = 0$; bursts vanish at $H = 15$ or so while gusts last even when H is more than 30. For the case of temperature, the structure is different; for neutral conditions, it appears that gusts are equal to bursts too, but, as instability increases, bursts exceed gusts significantly (Run 120).

So far, there are not many published results with which to compare these

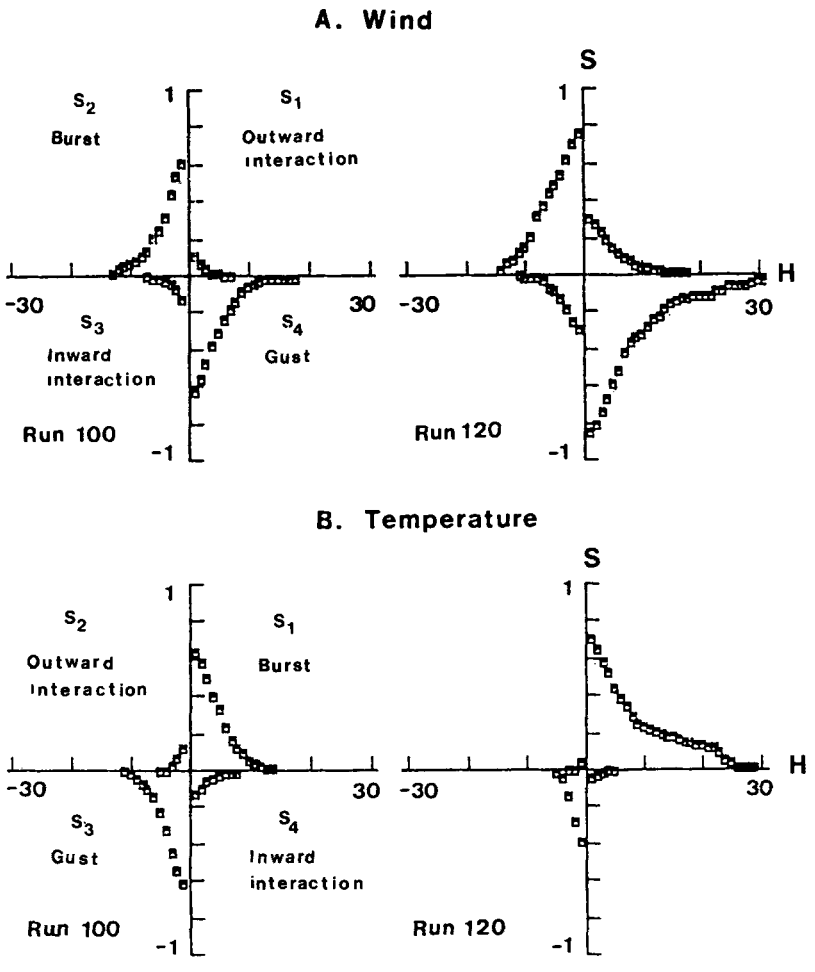

Fig. 11. The normalized contributions of s_i to $\overline{u'w'}$ (a) and $\overline{w'\vartheta'}$ (b) against the hole sizes H, for neutral (Run 100) and unstable (Run 120) conditions.

observations. Finnigan (1979) analyzed the four quadrant distributions and their variations with height up to 2 m, from below to above the canopy in a 1.2 m high wheat crop field. He found that within and above the canopy, the resultant $u'w'$ is a relatively small difference between large negative and positive contributions from gusts and outward interactions, respectively. Within the canopy, bursts and inward interactions are negligible; above the canopy, bursts start to increase in importance; large values of S_4 and S_1 reflect the increased intermittency of Reynolds stress arrivals, associated with a low mean wind speed. In the laboratory, Lu and Willmarth (1973) have established that the average frequency of gust arrival at the surface in a smooth-wall turbulent boundary layer can be scaled with mean velocity and boundary-layer thickness. Weiss and Allen (1976) measured

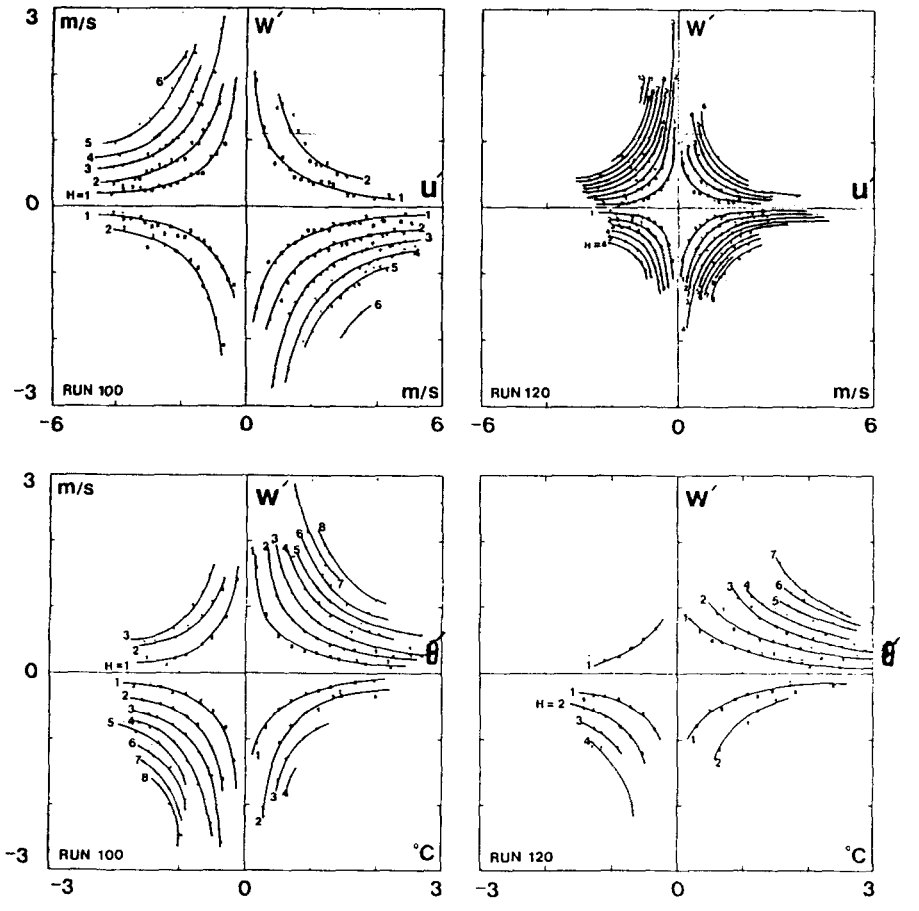

Fig. 12. The contours of the normalized contributions, $S_{i,H}$ to $\overline{u'w'}$ and $\overline{w'\vartheta'}$ from each quadrant as a function of different hole size for neutral (Run 100) and unstable (Run 120) conditions.

the flux angle distribution of momentum above 2 m high vine rows, and showed the relative intensity of gusts compared to bursts over their surface.

Some wind tunnel experiments show that gusts replace bursts as the principal mechanism of momentum transfer as a rough wall is approached and that this effect is more pronounced as the surface roughness increases (Nakagawa and Nezu, 1977). Raupach *et al.* (1980) also obtained similar results in a wind tunnel experiment in rough-wall and smooth-wall turbulent boundary layers. They found that bursts occupied most of the boundary layer, but gusts accounted for most of the stress close to rough surfaces. The relative magnitude of the gust component increased both with surface roughness and with proximity to the surface; and the gust-dominated region delineated the roughness sublayer to a depth of up to several roughness element heights. This implies that the equality of gusts and

bursts should appear near the top of the roughness sublayer. In the present study over the mallee-bush rough surface, the equality of gusts with bursts was observed for both momentum and temperature under neutral conditions, and this result was obtained at a height of 8.4 m above ground, where the eddy correlation measurements were made. Coincidently, this height was just around the top of the roughness sublayer, 8–10 m (about 4 times the canopy height), under neutral conditions as demonstrated by Chen (1987), and Chen and Schwerdtfeger (1989). However, temperature bursts predominate over gusts most of the time in unstable conditions, which implies that heat transfer has a different mechanism than momentum.

As a quantitative measure of the relative importance of these two types of event, Raupach (1981) suggested consideration of only the differences of contribution S:

$$\begin{aligned} \Delta S_{H,M} &= S_{4,H} - S_{2,H} \quad \text{for momentum} \\ \Delta S_{H,T} &= S_{3,H} - S_{1,H} \quad \text{for temperature,} \end{aligned} \tag{7}$$

where $\Delta S_{H,M}$ is the difference of contributions S between quadrants 4 and 2 for momentum at a hole size of H, while $\Delta S_{H,T}$ is the difference of contributions S between quadrants 3 and 1 for temperature at a hole size of H. Obviously, for a dominance of gusts, it would be expected that $\Delta S > 0$, and for bursts, $\Delta S < 0$; Raupach (1981) also demonstrated that ΔS for momentum is closely related to the third moments of the streamwise and normal velocity fluctuations, u' and w', which can be derived by a cumulant-discard method (Antonia and Atkinson, 1973; Nakagawa and Nezu, 1977); in the case of $H = 0$, specifying the difference between all stress contributions in the gust and burst quadrants, $\Delta S_{H,M}$ can be expressed as

$$\Delta S_{0,M} = \frac{1+\beta}{\beta\sqrt{2\pi}}\left(\frac{2C_1}{(1+\beta)^2} + \frac{C_2}{1+\beta}\right) \tag{8}$$

where,

$$C_1 = (1+\beta)(\tfrac{1}{6}(M_{03} - M_{30}) + (M_{21} - M_{12})) \tag{9}$$

$$C_2 = -(\tfrac{1}{6}(2-\beta)(M_{03} - M_{30}) + (M_{21} - M_{12})) \tag{10}$$

where β is the correlation coefficient, defined as $\overline{u'w'}/(\sigma_u\sigma_w)$; here σ denotes a standard deviation, and M represents the third moments ($M_{30} = \overline{u'u'u'}$, $M_{03} = \overline{w'w'w'}$, $M_{12} = \overline{u'w'w'}$, $M_{21} = \overline{u'u'w'}$). Figure 13 shows $\Delta S_{0,M}$ against the third moment for the entire experimental data set. Obviously, $\Delta S_{0,M}$ is well correlated with M_{03}, M_{12} or M_{31}; however, the relation with M_{30} is more scattered. To verify these relationships, observed values of $\Delta S_{0,M}$ have also been plotted against the computed values from formula (8) for the 250 runs (Figure 14). Though a good linear relationship is found, the computed values are about 8 times greater than the observed ones.

The observed $\Delta S_{0,M}$ and $\Delta S_{0,T}$ have also been plotted against stability ζ for the 250 runs, as shown in Figures 15a and b, respectively; for momentum, the points

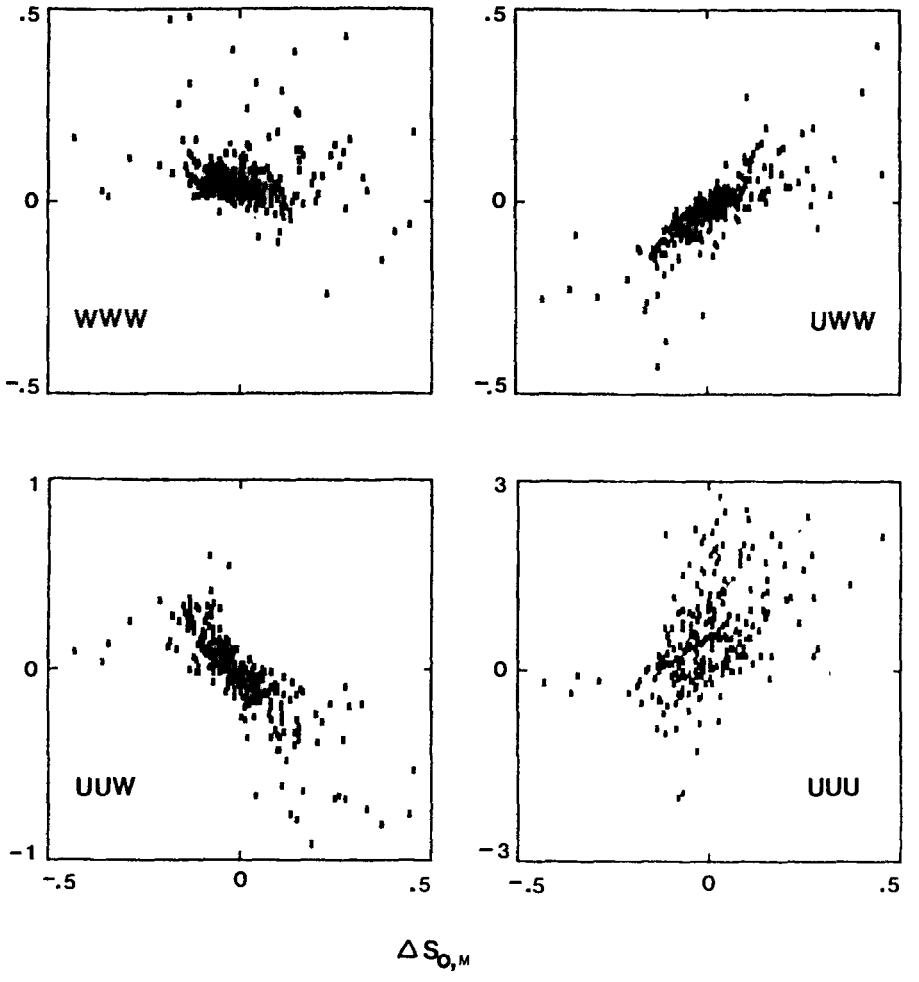

Fig. 13. Relations of parameter $\Delta S_{0,H}$ with the third moments of *www*, *uww*, *uuw*, and *uuu*.

are almost equally distributed around the line $\Delta S_{0,M} = 0$ throughout the range of stability; this is not surprising in the light of the results of Figure 11a where the behaviour of S_4 matches that of S_2 both in neutral and unstable conditions; for temperature, $\Delta S_{0,T}$ decreases with increasing instability and becomes negative, which implies a predominance of burst events as also shown in Figure 11b.

The joint probability density functions of u' or ϑ' with w', $P(u', w')$ or $P(\vartheta', w')$ are also presented, because they are related to the behavior of the quadrant contribution $S_{i,H}$, i.e., the contribution fraction in the ith quadrant with a specified hyperbolic hole region of size H, defined as

$$S_{i,H} = (\widehat{u'w'})_{i,H}/\overline{u'w'} \qquad \text{for momentum}$$

$$S_{i,H} = (\widehat{\vartheta'w'})_{i,H}/\overline{u'w'} \qquad \text{for temperature.}$$

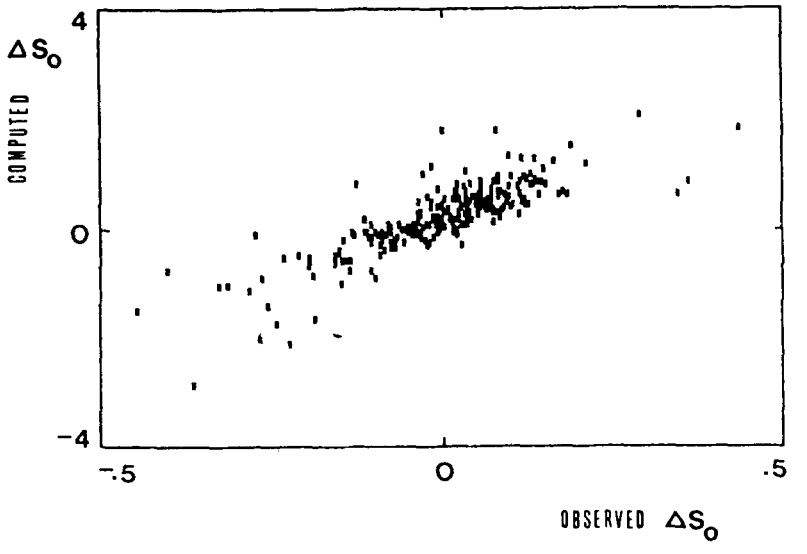

Fig. 14. Comparison of the observed parameter ΔS_0 with the theoretically computed.

Here, the angle bars denote a conditional average. For momentum $S_{i,H}$ can be precisely written as (Raupach, 1981)

$$S_{i,H} = \frac{1}{\beta} \int_{-\infty}^{\infty} \int_{-\infty}^{\infty} \hat{u} \cdot \hat{w} \cdot P(\hat{u}, \hat{w}) \cdot I_{i,H}(\hat{u}, \hat{w}) \cdot \mathrm{d}\hat{u}\, \mathrm{d}\hat{w} \tag{11}$$

where β is the correlation coefficient as defined before, $\hat{u}, \hat{w}$ are the re-scaled velocity components:

$$\hat{u} = u'/\sigma_u \qquad \text{and} \qquad \hat{w} = w'/\sigma_w;$$

σ denotes the standard deviation, and the indicator function $I_{i,H}$ obeys the relationships:

$$I_{i,H}(\hat{u},\hat{w}) = \begin{cases} 1, & \text{if } (u',w') \text{ is in the } i\text{th quadrant} \\ & \text{and if } |u'w'| \geq H \cdot |\overline{u'w'}|, \\ 0, & \text{otherwise.} \end{cases}$$

Relationships similar to the above can be derived for temperature.

Figure 16 shows contours of $P(\hat{u},\hat{w})$ and $P(\hat{\vartheta},\hat{w})$ for wind and temperature, respectively. The contours of Run 100 for wind give a representative example that resembles the concentric ellipses of the joint Gaussian distribution and in which sweeps match bursts. As wind weakens and the atmosphere becomes more unstable, the most favored location for large values of $-u'w'$ tends to shift to the sweeps quadrant (Run 120). For the temperature case, the contours are not symmetrical about the origin in most conditions and bursts seem to outweigh

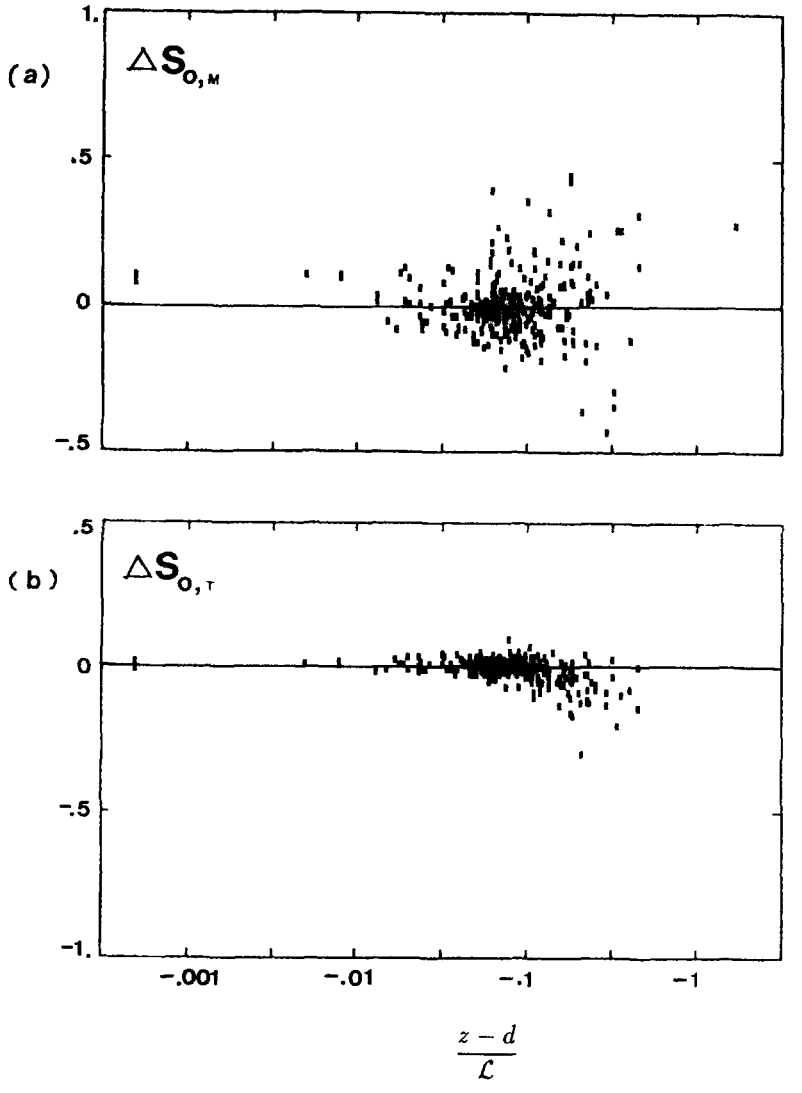

Fig. 15. The relative importance of gusts to bursts, parameter $\Delta S_{0,M}$ and $\Delta S_{0,H}$ for momentum and temperature, respectively, against stability.

sweeps; only for weak winds in neutral conditions do sweeps tend to match bursts or dominate slightly over them.

4. Conclusion

Large structures (bursts and sweeps) have been identified by means of spectral analyses and short-period space-time correlation methods, and it is found that

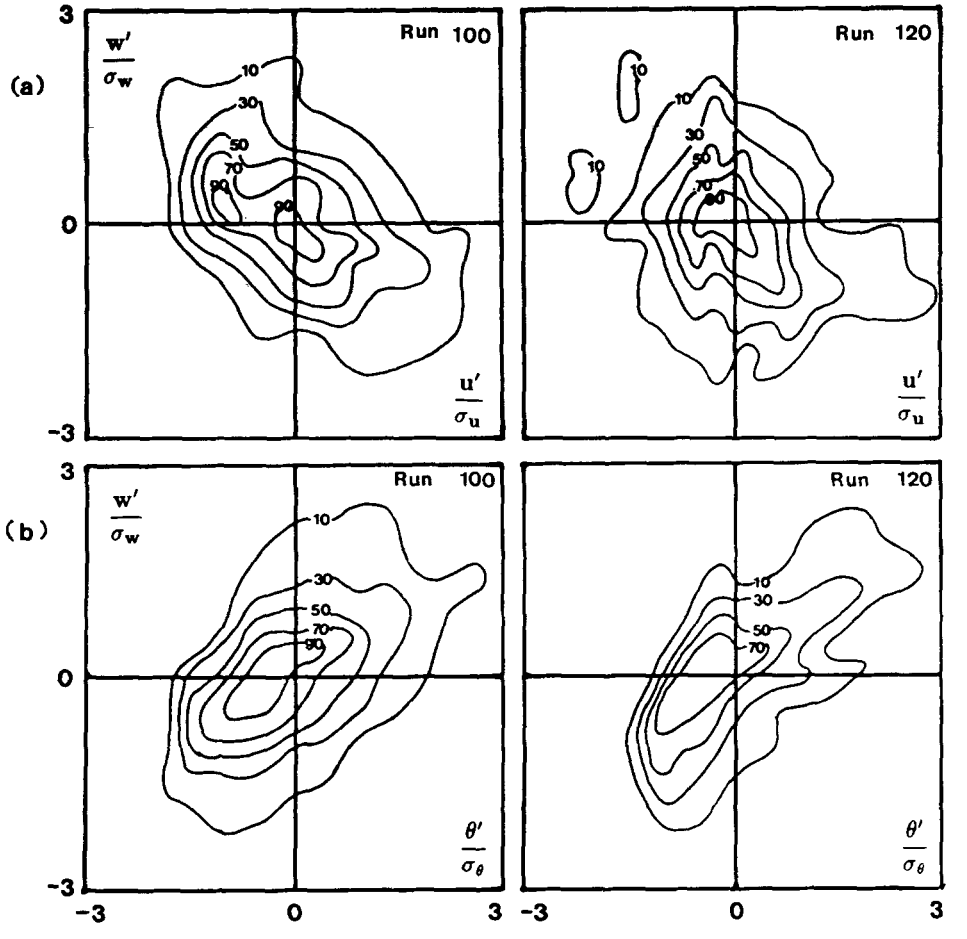

Fig. 16. The joint probability density functions, $P(\hat{u}, \hat{w})$ and $P(\hat{\vartheta}, \hat{w})$ for neutral (Run 100) and unstable (Run 120) conditions. Contours denote percentage values of probability.

they have time scales of 10–30 sec. Comparison with other results over relatively smooth surfaces indicates that the turbulent structures over rough surfaces have an inherently larger length scale. These length scales also increase with instability. It is, therefore, expected that this could result in much stronger turbulent mixing over rough surfaces, and the effects become even higher under unstable conditions. This has also been demonstrated by the finding that the depth of the roughness sublayer increases with instability. These effects also reach a very deep air layer (about 10 times the canopy height), which is much higher than expected from laboratory wake diffusion experiments (in general, only of the same order as the roughness height); wake diffusion has been widely considered as the main mechanism for the enhancement of turbulent mixing over rough surfaces. Thus, the

inherently larger structures over rough surfaces may result in a different process than that of simple generation of turbulence by plant wakes.

It was also noted that gusts or bursts often appear in a repeated sequence, rather than a gust immediately followed by a burst, which is often found in the laboratory.

The major fractions of heat and momentum fluxes are transferred by these large structures in a small fraction of the total time. The partition of the quadrant contributions of momentum and heat demonstrates that at the measurement height of the study (8.4 m, about four times the canopy height), bursts are approximately equal in strength to gusts under neutral conditions for either momentum or temperature transport. This should occur at the top of the roughness sublayer according to previous laboratory studies.

However, in unstable conditions the mechanisms for momentum transfer and for temperature transfer are different; in that case, gusts tend to be dominant for momentum transfer and bursts for heat transfer. This implies that the equilibrium level of bursts and gusts (the alternative definition of the depth of the roughness sublayer) should be lifted to a higher level; this has also been demonstrated by the Hincks experiment (Chen, 1987; Chen and Schwerdtfeger, 1989).

The dependence of the quantity ΔS, introduced to describe the predominance of gusts or bursts in the near-surface layer, upon the third moments has been verified with the experimental data in the case of momentum; predicted values of ΔS are well-correlated with observed ones. The behaviour of $\Delta S_{0,M}$ for momentum as a function of stability is found to be different from that of $\Delta S_{0,T}$ for temperature.

Acknowledgements

This work was supported by the scholarship fund of Flinders University of South Australia. The author thanks Prof. Schwerdtfeger, and Drs. M. R. Raupach, J. J. Finnigan, A. R. G. Lang and J. Bennett for their helpful advice during the study, constructive reading of the draft, and critical comments.

References

Antonia, R. A. and Atkinson, J. D.: 1973, *J. Fluid Mech.* **58**, 581.

Allen, L. H., Jr.: 1968, 'Turbulence and Wind Spectra Within a Japanese Larch Plantation', *J. Appl. Meteorol.* **7**, 73–78.

Bradley, E. F.: 1969, 'A Small Sensitive Anemometer System for Agricultural Meteorology', *Agric. Meteorol.* **6**, 185–193.

Chen, F.: 1987, 'Turbulent Transfer for Momentum and Heat over a Vegetated Rough Surface', Ph.D. thesis, Flinders University of South Australia.

Chen, F. and Schwerdtfeger, P.: 1989, 'Flux-gradient Relationships for Momentum and Heat over a Rough Natural Surface', *Quart. J. Roy. Meteorol. Soc.* **115**, 335–352.

Coppin, P. A.: 1979, 'Turbulent Fluxes over a Uniform Urban Surface', Ph.D. thesis, Flinders University of South Australia.

Denmead, O. T. and Bradley, E. F.: 1985, 'Flux-gradient Relationships in a Forest Canopy', in Hutchison, B. A. and Hicks, B. B. (eds.), *Forest-Atmosphere Interaction*, D. Reidel Publishing Company, Dordrecht, Holland, pp. 421–442.

Finnigan, J. J.: 1979, 'Turbulence in Waving Wheat: I. Mean Statistics and Honami: II. Structure of Momentum Transfer', *Boundary-Layer Meteorol.* **16**, 181–236.

Garratt, J. R.: 1978, 'Flux-Profile Relations above Tall Vegetation', *Quart. J. Roy. Meteorol. Soc.* **104**, 199–211.

Grass, A. J.: 1971, 'Structure Features of Turbulent Flow over Smooth and Rough Boundaries', *J. Fluid Mech.* **50**, 233–255.

Isobe, S.: 1972, 'A Spectra Analysis of Turbulence in a Corn Canopy', *Bull. Nat. Inst. Agric. Sci.* (Japan) Ser. A, No. 19, 101–112.

Kim, H. T., Kline, S. J., and Reynolds, W. C.: 1971, 'The Production of Turbulence Near a Smooth Wall in a Turbulent Boundary Layer', *J. Fluid Mech.* **50**, 133–160.

Kovasznay, L. S. G., Kibens, V., and Blackmelder, R. F.: 1970, 'Large-Scale Motion in the Intermittent Region of a Turbulent Boundary Layer', *J. Fluid Mech.* **41**, 283–325.

Kovasznay, L. S. G.: 1977, 'The Role of Large-Scale Coherence Structures in Turbulent Shear Flows', in *Proc. 5th Biennial Symp. on Turbulence*, Science Press, Princeton.

Lu, S. S. and Willmarth, W. W.: 1973, 'Measurements of the Structure of the Reynolds Stress in a Turbulent Boundary Layer', *J. Fluid Mech.* **60**, 481–511.

Nakagawa, H. and Nezu, I.: 1977, 'Prediction of the Contributions to the Reynolds Stress from Bursting Events in Open-Channel Flows', *J. Fluid Mech.* **80**, 99–128.

Nychas, S. G., Hershey, H. C., and Brodkey, R. S.: 1973, 'A Visual Study of Turbulent Shear Flows', *J. Fluid Mech.* **61**, 513–540.

Raupach, M. R.: 1976, 'Atmospheric Flux Measurements by Eddy Correlation', Ph.D. thesis, Flinders University of South Australia.

Raupach, M. R.: 1978, 'Infrared Fluctuation Hydrometry in the Atmospheric Surface Layer', *Quart. J. Roy. Meteorol. Soc.* **104**, 309–322.

Raupach, M. R.: 1979, 'Anomalies in Flux-Gradient Relationships over Forest', *Boundary-Layer Meteorol.* **16**, 467–486.

Raupach, M. R., Thom, A. S., and Edwards, I.: 1980, 'A Wind-Tunnel Study of Turbulent Flow Close to Regularly Arrayed Rough Surfaces', *Boundary-Layer Meteorol.*, **18**, 373–397.

Raupach, M. R.: 1981, 'Conditional Statistics of Reynolds Stress in Rough-Wall and Smooth-Wall Turbulent Boundary Layers', *J. Fluid Mech.* **108**, 363–382.

Schwerdtfeger, P.: 1976, 'Physical Principles of Micrometeorological Measurements', Elsevier, p. 71.

Schwerdtfeger, P.: 1985, in Natural History of Eyre Peninsula, 6: Climate, Published by the Royal Society of S.A. (Inc) 1985, pp. 89–100.

Seginer, I., Mulhearn, P. J., Bradley, E. F., and Finnigan, J. J.: 1976, 'Turbulent Flow in a Model Plant Canopy', *Boundary-Layer Meteorol.* **10**, 423–453.

Seginer, I. and Mulhearn, P. J.: 1978, 'A Note on Vertical Coherence Streamwise Turbulence Inside and Above a Model Canopy', *Boundary-Layer Meteorol.* **14**, 515–525.

Wallace, J. M., Eckelmann, H., and Brodkey, R. S.: 1972, 'The Wall Region in Turbulent Shear Flow', *J. Fluid Mech.* **54**, 39–48.

Weiss, A. and Allen, L. H. Jr.: 1976, 'The Flux-Angle Distribution of Momentum as Determined from Propeller Anemometer Measurements', *Quart. J. Roy. Meteorol. Soc.* **102**, 775–779.

Willmarth, W. W.: 1975, 'Structure of Turbulence in Boundary Layer', in C. S. Yih (ed.), *Advances in Applied Mechanics*, Vol. 15, Academic Press, New York, pp. 159–254.